RESEARCH PAPER

Numerical Modeling for Collapse Analysis of Cable-Stayed Bridges using the Improved Applied Element Method

Mohamed Magdi Abdelaziz[1] · Hany Ahmed El-Ghazaly[1] · Mohamed Sayed Gomaa[1]

Abstract

This work presents a novel numerical simulation of the collapse process of cable-stayed bridges based on the improved applied element method, which was originally developed as an effective numerical tool for large-scale framed structures under severe loading circumstances. For that, a straight spring element type is utilized for modeling the stay-cable with an equivalent modulus of elasticity that combines the effects of material and geometric deformation of the bridge cables. Moreover, the advantage of the multi-layered element type, which allows for the modeling of various rectangular or non-rectangular RC and composite sections without any complications, is utilized for modeling the pylon and the deck. The pretension forces in the cables are applied by adding an initial loading procedure in which the stay-cable is exposed to an initial strain to consider the effect of prestressing. The mass matrix is modified to include the stay-cable mass, which is lumped at the centroid of the elements connected by the stay-cable. The proposed modeling approach takes material and geometric nonlinearities into account for both the multi-layered element and the stay-cable. Verification examples are provided to examine the capability of the model. The comparison between the results of the proposed modeling technique and the finite element results has shown good agreement, highlighting the reliability of the proposed modeling technique. In addition, the developed tool is used to carry out collapse analysis of a cable-stayed bridge under a cable-loss scenario to examine the capability of the proposed technique.

Keywords Cable-stayed bridges · Stay-cable · Collapse analysis · Improved applied element method · Multi-layered element · Cable-loss

List of Symbols

a	Element length
A_{cb}	The cross-sectional area of the stay-cable
d_l^i	The distance served by the ith spring in the Lth layer
ε_{int}^k	Initial strain in the stay-cable
E_L	Young's modulus of the Lth layer
E_{cb}	Young's modulus of stay-cable
E_{eq}	Equivalent modulus of elasticity of the stay cable
G_L	Shear's modulus of the Lth layer
$(K_n^i)_L$	Normal stiffness of the spring i in the Lth layer
$(K_s^i)_L$	Shear stiffness of the spring i in the Lth layer
$(K_n^i)_c$	Normal stiffness of the stay-cable spring
L_{cb}	Horizontal projected length of the cable
$[M]$	The mass matrix
$[M_s]$	The structural mass matrix that represents the element's own weight
$[M_{ns}]$	The non-structural mass matrix
M_1	First diagonal element of the mass matrix
M_2	Second diagonal element of the mass matrix
M_3	Last diagonal element of the mass matrix which corresponds to the element polar moment of inertia about its centroid
T	The tension in the stay-cable
T_n^i	Thickness of the spring "i" for normal case
T_s^i	Thickness the spring "i" for shear case
W	The weight of the stay-cable per unit length
ρ_{cb}	The density of the stay-cable

✉ Mohamed Magdi Abdelaziz
   mma22@fayoum.edu.eg

[1] Faculty of Engineering, Fayoum University, Faiyum, Egypt

1 Introduction

Bridge collapse incidents have been recorded in recent years, resulting in serious economic and life losses. Throughout history, numerous bridges have collapsed for

a variety of reasons, which fall into two broad categories: natural factors and man-made factors. Natural hazards such as earthquakes, tsunamis, floods, mudslides, and hurricanes may all cause structural collapse. Engineers are fully aware of these phenomena, and incorporating natural activities into design procedures is a requirement of building code requirements. Although those codes are generally conservative, certain failures do occur. On the other hand, collapse of structures can be caused by a variety of purposeful or unintentional man-made hazards, including violent changes in air pressure caused by an explosion or blast, accidental collisions between vehicles and bridge superstructures, fire, and vehicle overloading. These incidents, however, are random in nature, depending on the significance and vulnerability of the target structure, ease of access, and other complicating variables (Deng et al. 2016).

Several studies on structural failures have been published in recent years, and considerable emphasis has been placed on buildings, leaving the bridge area unexplored or just partially studied. However, recent bridge failures in Genoa (Italy) in 2018, Kolkata (India) in 2018, and Su'ao Township (Taiwan) in 2019 have highlighted public concern about infrastructure safety due to their repercussions for lives and injuries, as well as economic and social losses (Domaneschi et al. 2019).

The collapse analysis of cable-stayed bridges was investigated under different loading scenarios. The unexpected loss of cables is typically coupled with both material and geometrical nonlinearities, resulting in significant impulsive dynamic loads on the structure that might potentially cause the entire bridge to collapse. Accordingly, the structural response of such bridges under the unexpected loss of cables was investigated by means of static and dynamic analyses (Wolff and Starossek 2009; Cai et al. 2012; Samali et al. 2015; Das et al. 2016a; Das et al. 2016b; Naji and Ghiasi 2019). Most of these studies were performed using the finite element method (FEM) employed in SAP2000 and ANSYS, and hence, no simulation of the collapse process was given. The cable loss was modeled in terms of load applications by generating an impact load on the pylon and the deck in the opposite direction. Conversely, different studies were conducted to study the response up to collapse of the cable-stayed bridges under various loading conditions. The torsional response of the Morandi Bridge under the removal of a cable-stay was studied by Scattarreggia et al. (2022). Both the FEM and the applied element method (AEM) were used to show the damage migration for different reinforcement layouts. Moreover, the bridge was studied under the impact of a falling object on a bridge deck (Scattarreggia et al. 2023). The AEM was selected to model the impact phenomena and the possibly ensuing progressive collapse scenarios. Numerous research focused on the same bridge in an effort to determine what caused its collapse (Domaneschi et al. 2020; Nuti et al. 2020; Malomo et al. 2020).

These investigations demonstrated the application of the AEM to track the bridge's behavior all the way to its total collapse.

A case study of a cable-stayed bridge under blast loading conditions was presented by Mudragada and Mishra (2021) to assess the bridge's resistance against the progressive collapse induced by localized failure. In this study, SAP2000 software was employed. Three different blast scenarios were considered to understand bridge performance under blast loads. According to the results, the bridge was found to be too weak to withstand the explosion loads at the tower position, and progressive collapse was unavoidable. The response of the bridge was presented in terms of hinge formation, maximum stresses, and joint displacements, and therefore, no collapse simulation was provided.

The collapse of the cable-stayed bridges under strong seismic excitations was investigated by Domaneschi et al. (2019); Wang et al. 2017) using the FEM employed in LS-DYNA software and the AEM employed in ELS software. From these studies, it was found that the piers and the main pylons were crucial components contributing to the collapse of the cable-stayed bridge structure. Moreover, the failure of more than two cables at mid-span during the earthquake might make the bridge incapable of sustaining without causing excessive collapse. The collapse simulation was given only for the study carried out by the AEM.

High-resolution FE explicit simulation was used to study the dynamic response of a long-span cable-stayed bridge with high-rise twin pylons under ship impact (Guo et al. 2020). In this study, the ship and bridge details were carefully taken into account. In addition, springs were utilized to consider the soil–pile interaction.

For better assessing the actual damage state of a long-span cable-stayed bridge, a nonlinear FE model updating-based collapse prediction approach was developed (Lin et al. 2021). The viability and accuracy of the suggested collapse prognosis approach are confirmed by comparing the simulation findings with practical observations and measurement data from the shaking table test. In this study, no collapse simulation process was provided. Moreover, a digital twin-based collapse fragility assessment technique was provided for long-span cable-stayed bridges during powerful earthquakes (Lin et al. 2021). In this study, three FE bridge models were created: a design-based model, a linear model, and a nonlinear model. For these models, the collapse fragility curves of each model were determined using incremental dynamic analysis. The proposed method was found to be practical and reliable for estimating the likelihood of the seismic collapse of such bridges.

A novel progressive seismic FE model was presented for RC cable-stayed bridges located in earthquake-prone areas

(Zheng et al. 2022). A series of shaking experiments were performed on a 1:12 scale reinforced concrete pedestrian cable-stayed bridge with increasing peak ground accelerations. The undamaged condition of the bridge was represented by a FE model, which was then nonlinearly updated according to the collected data from the measurement equipment when the bridge model was subjected to mild shaking table excitations. The observed results from the shaking table tests and the nonlinearly updated FE model were in good agreement.

Unlike previous models, the objective of the current work is to extend the IAEM, which was originally utilized for large-scale framed structures, to facilitate modeling the collapse mechanism of cable-stayed bridges. In brief, the AEM is a discretization method that reflects the continuity of the structure by connecting finite rigid components along their borders with unique springs. The IAEM developed the idea of the multi-layered cross section to increase the method's range of applications (Abdelaziz et al. 2023). The main distinction between the IAEM and the conventional AEM is that the AEM often employs a higher number of elements to model nonrectangular cross sections in order to follow the thickness change throughout the section height (Elkholy and Meguro 2004; El-Kholy et al. 2012). In contrast, the complete cross section may be modeled as one element utilizing the IAEM regarding all considerable non-homogeneous materials, resulting in a significant reduction in the amount of time and resources needed to solve the problem (Abdelaziz et al. 2021a). Although the IAEM showed good ability in the modeling of framed structures, it is limited in its ability to model some special structures, such as cable-stayed bridges. Therefore, the current work focuses on extending the approach to facilitate modeling the cable-stayed bridges.

2 Improved Applied Element Method (IAEM)

IAEM, a recently developed simulation tool, is used for modeling large-scale framed buildings with non-homogeneous cross sections, including RC and retrofitting sections, as well as bonded and unbonded structures (El-Kholy et al. 2012; Abdelaziz et al. 2021a, 2020, 2021b, 2022). This method has the ability to follow structural performance with great precision until the final collapse stage in a reasonable solving time.

In this approach, the structure is modeled as an assembly of multi-layered rigid elements linked together by nonlinear springs along the boundary line, representing axial and normal deformations.

These elements consist of several layers representing the unconfined and confined concrete, the bonded non-prestressing and prestressing reinforcement, and the retrofitting layer, as given in Fig. 1 (Abdelaziz et al. 2021a). Using the advantages of this element type, different cross-sectional shapes with various material types can be represented without difficulty. All similar layers in the neighboring elements are linked together by sets of normal and shear springs, representing the material characteristics of each layer as shown in Fig. 2 (El-Kholy et al. 2012). The normal and shear stiffness values $(K_n^i)_L$ and $(K_s^i)_L$ for each pair of springs in the Lth layer are as follows: (El-Kholy et al. 2012)

$$(K_n^i)_L = \frac{E_L . d_L^i . (T_n^i)_L}{a} \tag{1}$$

$$(K_s^i)_L = \frac{G_L . d_L^i . (T_s^i)_L}{a} \tag{2}$$

where the subscripts n and s denote normal and shear springs, respectively; E_L and G_L refer to the Young's and the shear's modulus of the Lth layer, respectively; d_l^i denotes the distance served by the ith spring in the Lth layer, T_n^i and T_s^i denote the thicknesses represented by the pair of springs "i" for normal and shear cases, respectively; and a is the length of the representative area.

Figure 3 shows the flowchart for the major component of the method. The structural equilibrium equation may be solved using both the load control and displacement control incremental methods. The softening behavior of the structures can also be tracked. The geometric nonlinearity algorithm is the same as the conventional AEM approach
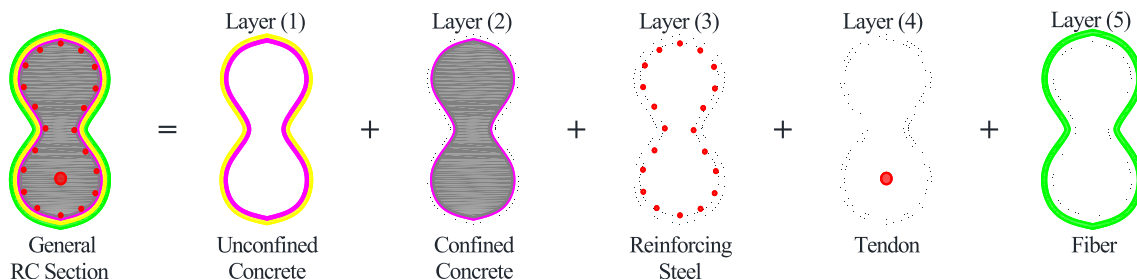

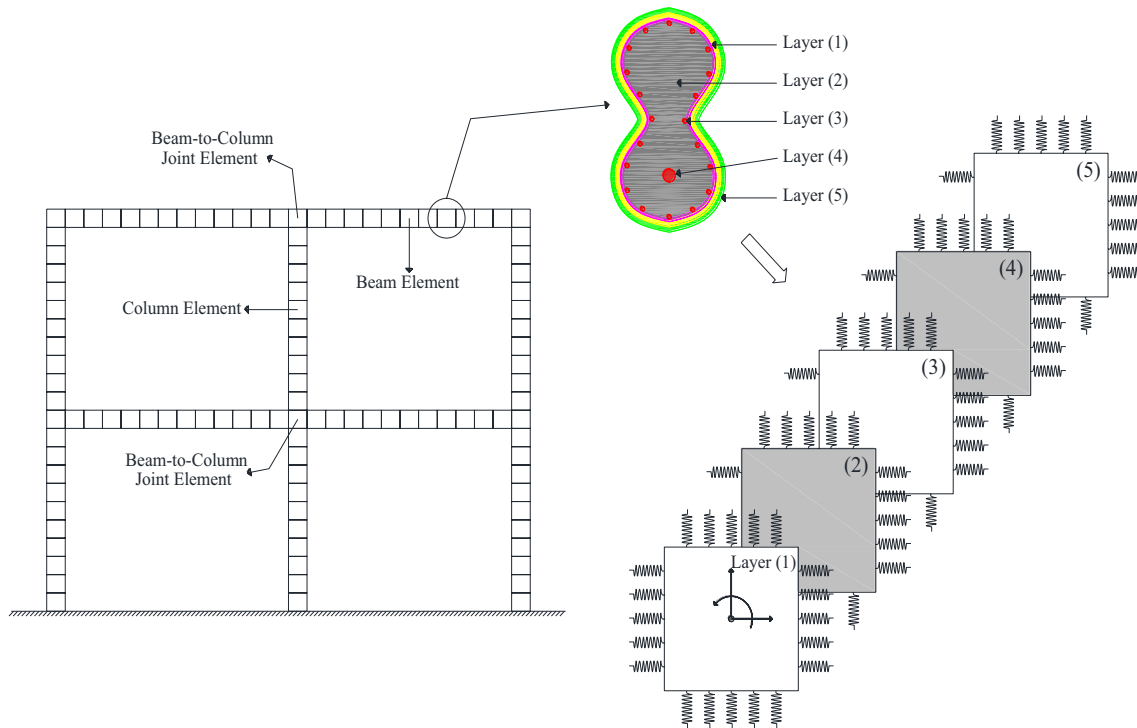**Fig. 1** The multi-layered element type (Abdelaziz et al. 2021a)

Fig. 2 Modeling RC framed structures with IAEM (Abdelaziz et al. 2021b)

(Meguro and Tagel-Din 2002), including P-effects and large displacement analysis.

3 IAEM Simulation of Cable-Stayed Bridge

A cable-stayed bridge's superstructure is typically composed of three major structural components: pylons, inclined stay-cables, and the bridge deck. These structural components can be made of different materials. As a result, a long-span cable-stayed bridge is frequently a complicated structure composed of different materials. In the proposed modeling technique, pylons and decks are modeled using the advantage of the multi-layered element type, which consists of several layers representing homogeneous or non-homogeneous cross sections. Various rectangular or non-rectangular RC and composite sections can be modeled using large size elements without any complications, resulting in an accurate simulation of these large scale structures with a reasonable solving time and computer resources.

The stay-cable, on the other hand, is represented as a straight spring element type with an equivalent modulus of elasticity that takes into account the effects of material and geometric deformation of the bridge's cables, as shown in Fig. 4. All cables are pinned to the pylon and to the deck at their points of attachment. In reality, a stay-cable will sag into a catenary shape according to its weight and tensile force.

Given that the stay-cable is modeled as a straight segment, the sag effect has to be considered using the equivalent modulus of elasticity of the stay-cable (E_{eq}), which can be determined as:

$$E_{eq} = \frac{E_{cb}}{1 + \frac{(wL_{cb})^2 A_{cb} E_{cb}}{12 T^3}} \tag{3}$$

where E_{cb} is the stay-cable's modulus of elasticity, w is the stay-cable's weight per unit length, L_{cb} is the stay-cable's horizontal projected length, A_{cb} is the stay-cable's cross-sectional area, and T is the tension in the stay-cable. This concept was first suggested by Ernst (Ernst 1965). The modulus of elasticity of the stay-cable (E_{cb}) is calculated in each loading step according to the strain in the cable, the loading or unloading state, and the spring's past history, and as a result, the equivalent modulus of elasticity is updated in each loading step. The normal stiffness $(K_n^i)_c$ of the spring representing a stay-cable can be determined as:

$$(K_n^i)_c = \begin{cases} [\frac{E_{eq}^i \cdot A_{cb}^i}{l_{cb}^i}], u_1 > 0 \\ \\ [0], u_1 \leq 0 \end{cases} \tag{4}$$

where E_{eq}^i is equivalent modulus of elasticity of the ith stay-cable determined in Eq. (3); A_{cb}^i is the cross-sectional area of the ith cable; l_{cb}^i is the representative length of the ith

Fig. 3 Flow chart of the IAEM (El-Kholy et al. 2012)
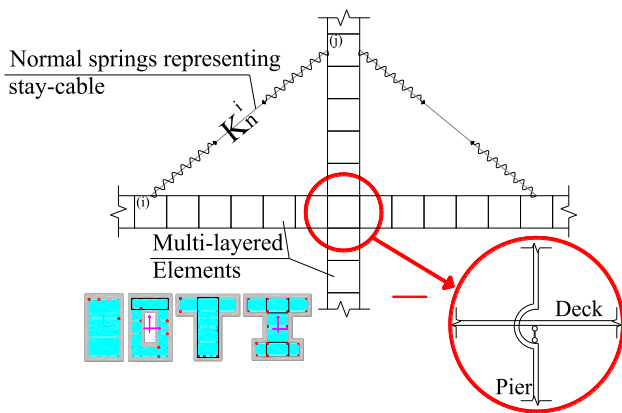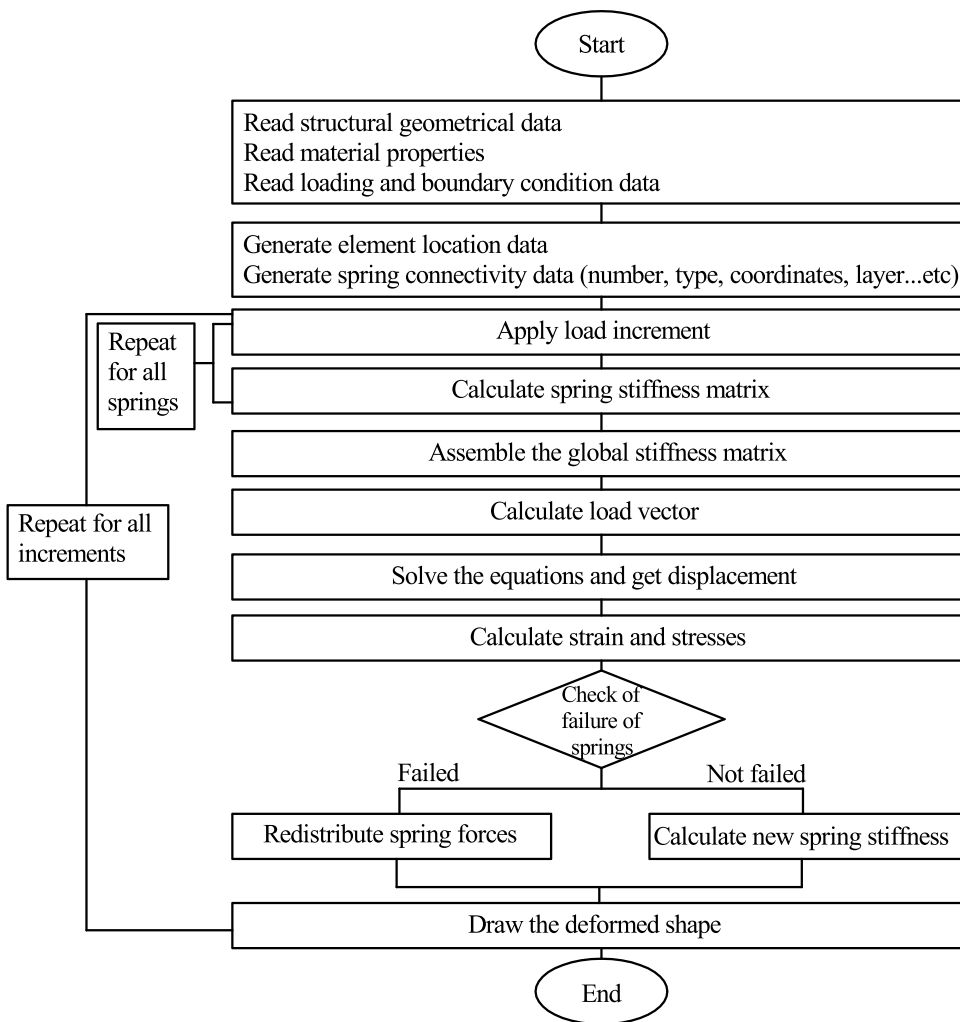
Fig. 4 Generation of springs representing the stay-cable

The cables' pretension forces are applied by adding an initial loading process in which the stay-cables' springs are exposed to an initial strain to account for the effect of pre-stressing. The initial strain for the cable springs ($\varepsilon_{\text{int}}^c$) can be determined as follows:

$$\varepsilon_{\text{int}}^c = \frac{\sigma_{\text{cb}}}{E_{\text{cb}}} \tag{5}$$

where σ_{cb} is the prestressing stress in the stay-cable.

A new connection element type has also been included to simulate the pylon-deck connection. This element type generates vertical links that enable the transmission of axial loads from deck to pier without moment transfer, as indicated in Fig. 4.

3.1 Local Stiffness Matrix Formulation

The local stiffness matrix for only one pair of contact springs in each multi-layered element is computed by assuming a

cable; and u_1 is the relative axial deformation. This equation shows that the normal springs representing stay-cables are assumed to resist only tensile forces.

unit displacement in each degree of freedom. The upper left quarter components of the matrix are given in Eq. (6) (Abdelaziz et al. 2021a). On the other hand, the local stiffness matrix of the normal springs, which represent the stay-cable, is given in Eq. (7). All notations used in this equation are depicted in Fig. 5. It should be noted that the stiffness matrix has the complete effect from all of the pairs of springs depending on the stress condition around the element. The stiffness matrices of individual springs at each layer, as well as the stiffness matrices of the stay-cable springs, are summed to form the multi-layered element's condensed stiffness matrix. The global stiffness matrix of the structure is then computed by summing the global stiffness matrices of the elements.

$$
\begin{bmatrix} M_1 \\ M_2 \\ M_3 \end{bmatrix} = \begin{bmatrix} \frac{a}{nsp} \times \sum_{i=1}^{i=nsp} \sum_{j=1}^{j=nlyr} \rho_j b_i t_j^x \\ \frac{a}{nsp} \times \sum_{i=1}^{i=nsp} \sum_{j=1}^{j=nlyr} \rho_j b_i t_j^y \\ \sum_{i=1}^{i=nsp} \frac{a^3 \times \sum_{j=1}^{j=nlyr} \rho_j b_i t_j^x}{12 \times nsp^2} + \frac{a \times \sum_{j=1}^{j=nlyr} \rho_j b_i^3 t_j^y}{12 \times nsp^2} \end{bmatrix} \tag{9}
$$

where a is the element length, nsp and nlyr are the number of connecting springs and layers, respectively, ρ_j is the material density of the jth layer, b_i is the width served by the spring in the jth layer, and t_j^x and t_j^y are the ith spring's thicknesses in the jth layer in the x and y directions, respectively (El-Kholy et al. 2012).

The structure's global mass matrix is determined by adding the local mass matrices of all the elements taken into

$$
\begin{bmatrix} \sin^2(\theta+\alpha)K_n^i & -K_n^i\sin(\theta+\alpha)\cos(\theta+\alpha) & \cos(\theta+\alpha)K_s^i L\sin(\alpha) \\ +\cos^2(\theta+\alpha)K_s^i & +K_s^i\sin(\theta+\alpha)\cos(\theta+\alpha) & -\sin(\theta+\alpha)K_n^i L\cos(\alpha) \\ -K_n^i\sin(\theta+\alpha)\cos(\theta+\alpha) & \sin^2(\theta+\alpha)K_s^i & \cos(\theta+\alpha)K_n^i L\cos(\alpha) \\ +K_s^i\sin(\theta+\alpha)\cos(\theta+\alpha) & +\cos^2(\theta+\alpha)K_n^i & +\sin(\theta+\alpha)K_s^i L\sin(\alpha) \\ \cos(\theta+\alpha)K_s^i L\sin(\alpha) & \cos(\theta+\alpha)K_n^i L\cos(\alpha) & L^2\cos^2(\alpha)K_n^i \\ -\sin(\theta+\alpha)K_n^i L\cos(\alpha) & +\sin(\theta+\alpha)K_s^i L\sin(\alpha) & +L^2\sin^2(\alpha)K_s^i \end{bmatrix} \tag{6}
$$

$$
\begin{bmatrix} \cos^2\beta(K_n^i)_c & \cos\beta\sin\beta(K_n^i)_c & -\cos\beta L_1\sin(\theta_1-\beta)(K_n^i)_c \\ \cos\beta\sin\beta(K_n^i)_c & \sin^2\beta(K_n^i)_c & -\sin\beta L_1\sin(\theta_1-\beta)(K_n^i)_c \\ -\cos\beta L_1\sin(\theta_1-\beta)(K_n^i)_c & -\sin\beta L_1\sin(\theta_1-\beta)(K_n^i)_c & L_1^2\sin^2(\theta_1-\beta)(K_n^i)_c \end{bmatrix} \tag{7}
$$

3.2 Modification of the Mass Matrix

In addition to the elements' own weight and the non-structural masses, the stay-cable mass must be considered to present the essential characteristics of a cable-stayed bridge. The cable mass is lumped at the centroid of the elements that the stay-cable connects. The diagonal vector of the cable mass matrix $[M_c]$ can be determined as follows:

$$
[M_c] = \frac{\rho_{cb} A_{cb} L_{cb}}{2} \begin{bmatrix} 1 \\ 1 \\ 0 \end{bmatrix} \tag{8}
$$

where ρ_{cb} is the mass density of the cable, A_{cb} is the cross-sectional area of the cable, and L_{cb} is the representative length of the cable. In addition, the diagonal elements of the mass matrix for the multi-layered element are determined as follows:

account as follows:

$$
[M] = [M_s] + [M_{n.s}] + [M_c] \tag{10}
$$

where $[M_s]$ is the structural mass matrix that represents the element's own weight, $[M_{n.s}]$ is the non-structural mass matrix, and $[M_c]$ is the structural mass matrix of the stay-cable. It should be noted that the matrix $[M_c]$ only returns to the elements that are connected by the cable. These matrices can be described by the following equation:

$$
[M] = \begin{bmatrix} M_1 & 0 & 0 \\ 0 & M_2 & 0 \\ 0 & 0 & M_3 \end{bmatrix} \tag{11}
$$

where M_1 and M_2 are the additional masses applied at the translational DOFs of a certain element, and M_3 is the additional mass applied at the rotational DOF of the same element.

3.3 Material Modeling

The tangential stiffness of each spring depends on its material type, the loading or unloading stage, the strain of the spring, and the spring's past history. The Okamura and Maekawa compression model (Okamoto and Maekawa 1991), depicted in Fig. 6, is employed for both confined and
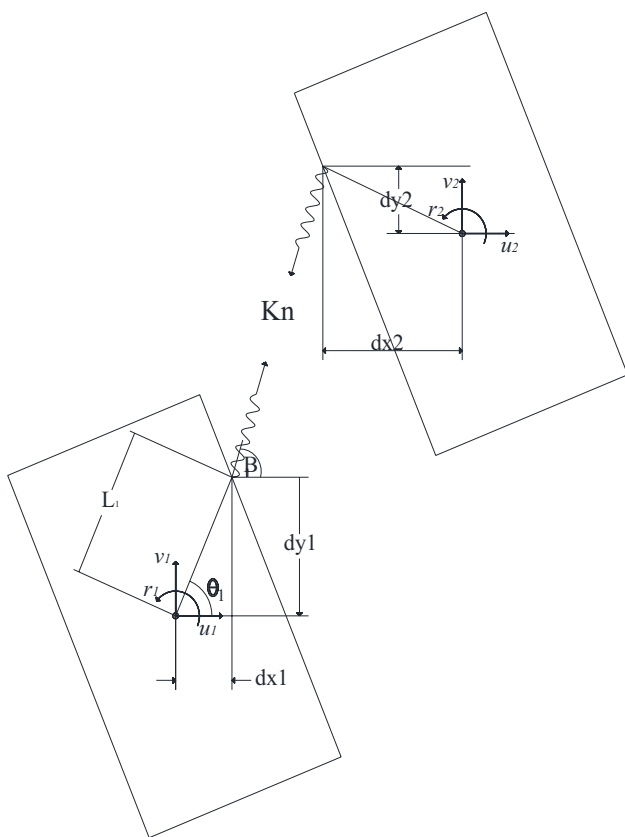
Fig. 5 Contact points and DOF for normal spring representing stay-cable

unconfined concrete springs. The tangent modulus of each concrete spring is computed at each load step, whether the concrete spring is in the loading or unloading stage. To avoid singularity, the spring stiffness is reduced to 1% of its initial value when the spring stress exceeds the compressive strength of concrete (El-Kholy et al. 2012). The stress–strain relationship for concrete under tension is considered to be linear, with the same initial stiffness until reaching the tensile strength of concrete. After cracking, the stiffness of

springs under tension is assumed to be zero. On the other hand, two material models may be used for steel springs and cable springs: the bilinear stress–strain model with kinematic strain hardening and the Menegotto and Pinto stress–strain model (Menegotto and Pinto 1973), which are depicted in Fig. 6. The Menegotto–Pinto model is recommended for higher numerical stability under complicated loading histories as it accounts for the effects of partial unloading and Bauschinger's effect.

4 Verification

To assess the method's capability for modeling cable-stayed bridges and its accuracy and reliability, two different verification examples of cable-stayed bridges have been modeled. The analysis results are compared to earlier research works and the FE analysis, which has been performed using the well-known FE program SAP2000 v.20 (CSI (Computers and Structures Inc.) 2020).

4.1 Static Analysis of Cable-Stayed Bridge (CSB#1)

This example presents a cable-stayed bridge model proposed by Cheung et al. (Cheung et al. 1996). The bridge has a center span of 400 m and two side spans of 160 m each. The deck girder is simply supported at the end abutments. Figure 7 shows the general configuration of this bridge model. Table 1 shows the cross-sectional properties of each component of the bridge model. Dead load is considered assuming a uniform D.L. of 10 t/m on the girder. In this load case, the pretension cable loads are computed by the rigid support method, and linear behavior is assumed. The prestressing forces in the cables are given in Table 2.

The bridge has been modeled in both IAEM using only 460 elements, as shown in Fig. 8, and FEM. The bending moment results of CSB#1 obtained using IAEM and FEM, as well as those obtained by Cheung et al. (Cheung et al. 1996), using the finite strip analysis are presented in Fig. 9.
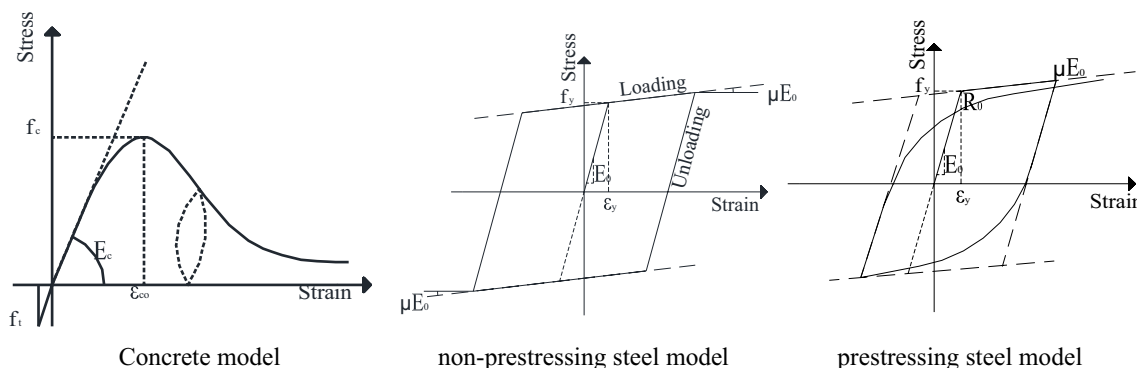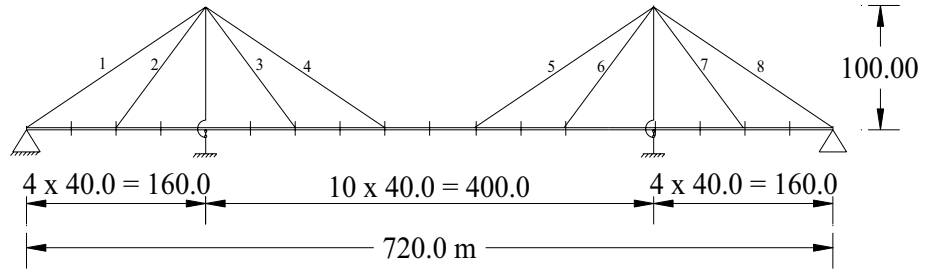

Fig. 6 Material model for concrete, non-prestressing steel, and prestressing steel (Abdelaziz et al. 2021a)

Fig. 7 General configuration of CSB#1

4 x 40.0 = 160.0   10 x 40.0 = 400.0   4 x 40.0 = 160.0

720.0 m

100.00

Table 1 Main data of bridge CSB#1

Member	Area (m²)	Moment of inertia (m⁴)	Modulus of elasticity (t/m²)
Girder	2.00	1.00	20.0×10^6
Cables 1, 4, 5, 8	0.10	–	15.2×10^6
Cables 2, 3, 6, 7	0.05	–	15.2×10^6
Pylon	20.00	5.00	20.0×10^6

⁻Not applicable

Table 2 Prestressing forces in various cables

Element ID	Prestressing forces (t)
1 & 8	1411.30
2 & 7	1161.65
3 & 6	1031.30
4 & 5	1499.63

Fig. 8 IAEM model for CSB#1

From the figure, it can be seen that the model's results can be categorized as satisfactory. Small differences have been identified. This, however, is still within the acceptable range.

4.2 Dynamic Analysis of a Fan-Shaped Cable-Stayed Bridge (CSB#2)

The second example presents a cable-stayed bridge with a configuration close to an existing bridge in Japan (the Meiko-Nishi Bridge in Nagoya) with a few modifications in dimensions. The bridge geometry is illustrated in Fig. 10, and the properties are given in Table 3. The static and dynamic behaviors of this bridge have been studied earlier by several other investigators (Abdel-Ghaffar and Nazmy 1991). The bridge has been modeled using IAEM as shown in Fig. 11. In the model, the girder has been pinned at the ends and connected to the pylons by vertical links. Furthermore, the pylons have been assumed to be rigidly fixed at their bottom ends.
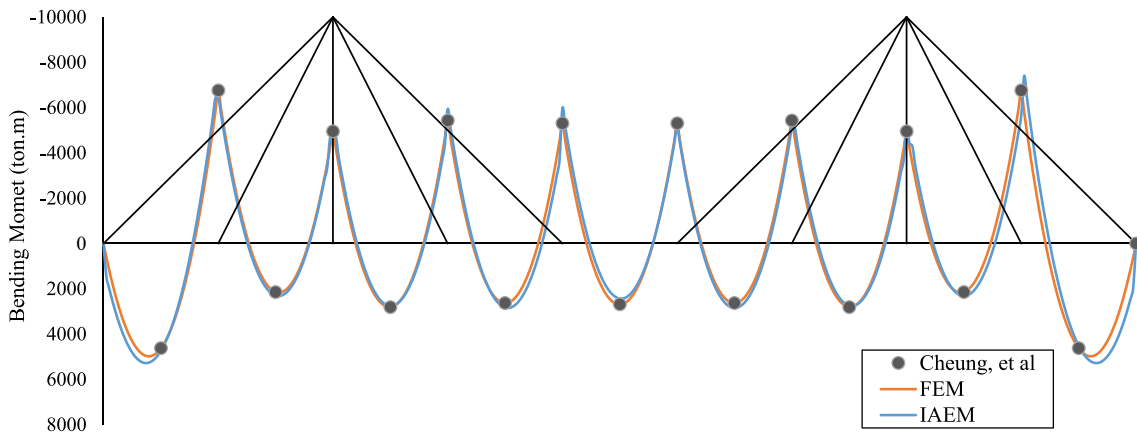

Fig. 9 Bending moment diagram of bridge model of CSB#1
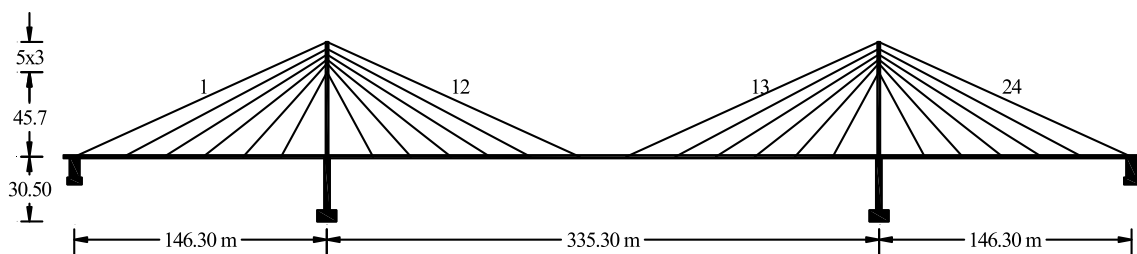
Fig. 10 General configuration of CSB#2

Table 3 Main data of bridge CSB#2

Member	Area (m^2)	Moment of inertia (m^4)	Modulus of elasticity (N/m^2)	Mass (t/m)
Girder	0.93	0.26	2.0×10^{11}	19.64[a]
Girder, central part	1.11	1.29	2.0×10^{11}	19.64[a]
Pylon above deck level	13.01	34.52	2.8×10^{10}	30.65
Pylon below deck level	18.58	86.31	2.8×10^{10}	43.78
Links, deck to pylons	0.56	–	2.0×10^{11}	4.38
Cables 1,24	0.0362	–	2.0×10^{11}	0.398
Cables 2, 11, 14, 23	0.0232	–	2.0×10^{11}	0.255
Cables 3, 10, 15, 22	0.0204	–	2.0×10^{11}	0.225
Cables 4, 9, 16, 21	0.0176	–	2.0×10^{11}	0.194
Cables 5, 8, 17, 20	0.0139	–	2.0×10^{11}	0.153
Cables 6, 7, 18, 19	0.0113	–	2.0×10^{11}	0.125
Cables 12, 13	0.0372	–	2.0×10^{11}	0.409

– Not applicable, [a]Including weight of cross-beams

Fig. 11 IAEM model for CSB#2
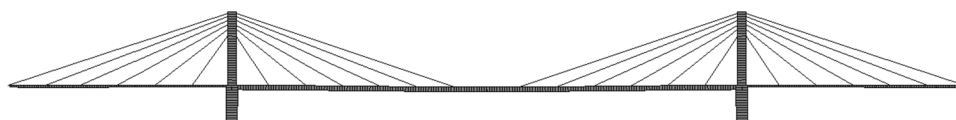
Modal analysis has been carried out to find the vibration properties, natural modes, and natural frequencies of the bridge to evaluate the method's capability for modeling cable-stayed bridges. The results are compared with the values obtained by Abdel-Ghaffar and Nazmy (1991) and with the values obtained by the finite element employed in SAP2000 software. The lowest vertical bending modes of vibration and the corresponding natural frequencies of the bridge are shown in Table 4.

According to this table, it can be observed that the IAEM manages to describe the mode shapes and the corresponding natural frequencies with good accuracy. Small differences are identified. However, this is still within an acceptable range.
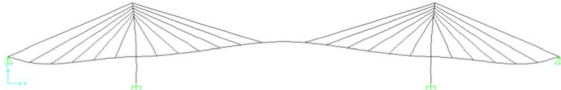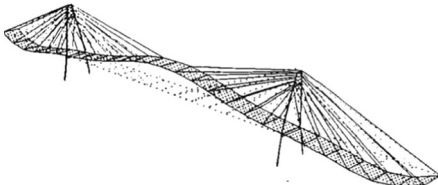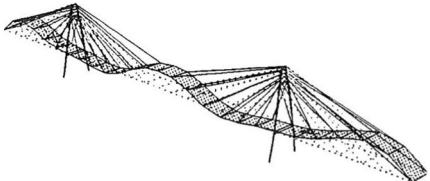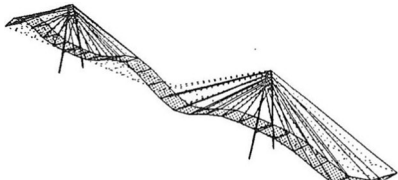
5 Cable-Stayed Bridge under Cable Loss
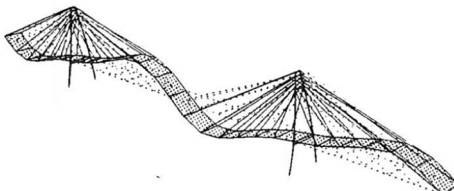
In order to examine the capability of the proposed technique, a cable-stayed bridge has been analyzed under a cable-loss scenario. The structure considered in this analysis has the same geometric dimensions as the cable-stayed bridge CSB#2 depicted in Sect. 4.2, with modifications in the cross-sectional properties of the bridge components to make the bridge much more vulnerable to collapse under cable-loss conditions. The properties of the proposed bridge are given in Table 5.

In the proposed method, the structure's design load as well as the prestressing forces in the cables are applied as initial loads, while the sudden loss of the cable element is applied as loading in the time domain. Once the loss of the cable occurs, the cable force is redistributed in the next increment by applying this force in the reverse direction. These redistributed forces are transferred to the element center as a force and a moment, and then, these redistributed forces are applied to the structure in the next increment.

The current study investigates the scenario of the simultaneous loss of two cables (11 and 12) in 0.20 s. The time step is set to 0.01 s. The deck and pylon are assumed to have a yield strength of 360 MPa. On the other hand, the

Table 4 First four natural modes of CSB#2

	Method	Mode	f(HZ)
1st mode	IAEM		0.3097
	FEM		0.3293
	Abdel-Ghaffar (1991)		0.3109
2nd mode	IAEM		0.43551
	FEM		0.4634
	Abdel-Ghaffar (1991)		0.4105
3rd mode	IAEM		0.66513
	FEM		0.6676
	Abdel-Ghaffar (1991)		0.6498
4th mode	IAEM		0.7199
	FEM		0.7389
	Abdel-Ghaffar (1991)		0.6994

Table 5 Main data of the proposed bridge

| Member	Area (m²)	Moment of inertia (m⁴)	Modulus of elasticity (N/m²)	mass (t/m)
Girder	0.2325	0.065	2.0×10^{11}	19.64[a]
Girder, central part	0.2775	0.3225	2.0×10^{11}	19.64[a]
Pylon above deck level	1.821	4.833	2.0×10^{11}	30.65
Pylon below deck level	2.601	12.083	2.0×10^{11}	43.78
Links, deck to pylons	0.56	–	2.0×10^{11}	4.38
Cables 1,24	0.0362	–	2.0×10^{11}	0.398
Cables 2, 11, 14, 23	0.0232	–	2.0×10^{11}	0.255
Cables 3, 10, 15, 22	0.0204	–	2.0×10^{11}	0.225
Cables 4, 9, 16, 21	0.0176	–	2.0×10^{11}	0.194
Cables 5, 8, 17, 20	0.0139	–	2.0×10^{11}	0.153
Cables 6, 7, 18, 19	0.0113	–	2.0×10^{11}	0.125
Cables 12, 13	0.0372	–	2.0×10^{11}	0.409

– Not applicable, [a]Including weight of cross-beams

**Fig. 12** Collapse mechanism of the cable-stayed girder due to cable loss
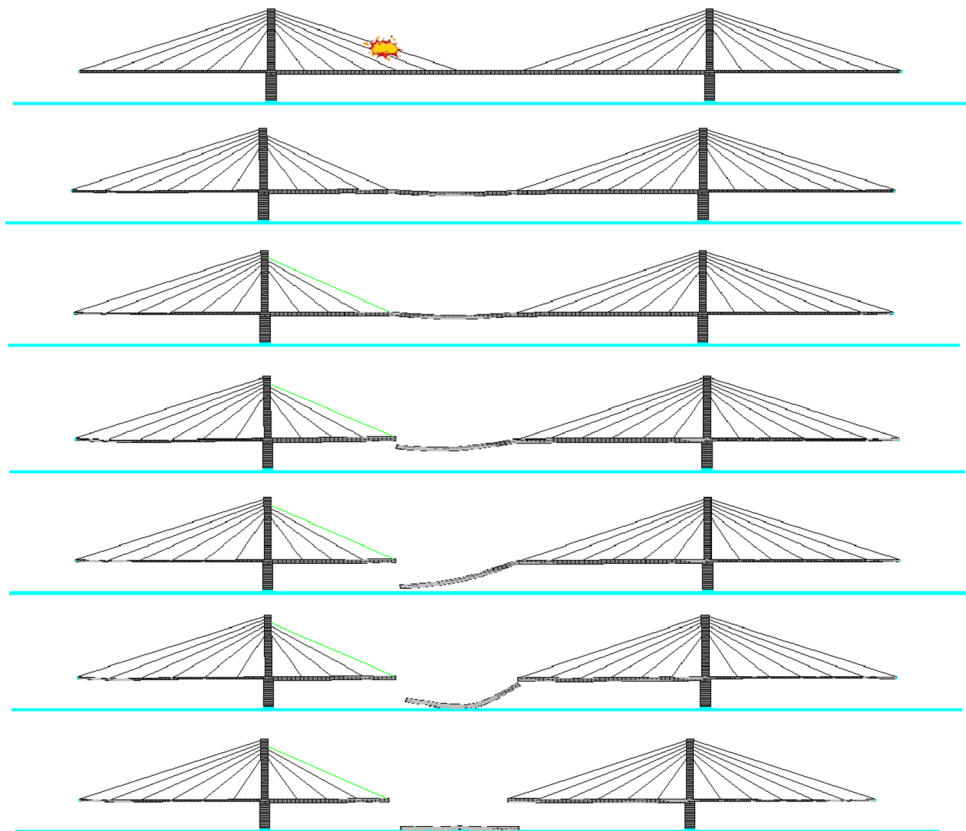
cables' yield strength is assumed to be 1550 MPa. IAEM has been used to perform a dynamic nonlinear collapse analysis. According to the simulation results, the mechanism of failure is shown in Fig. 12. Additionally, Fig. 13 displays the time history of the stress in cable 10. Moreover, the time-history of displacement at the extremities of both portions of non-collapsed decks are shown in Fig. 14. It should be noted that the positive displacement indicates downward movement of the bridge deck. The failure history can be summarized as follows:

1. When both cables have failed at the same time, an immediate push on the anchorage points on the pylon and the deck has been generated. The girder between cables 10 and 13 has experienced severe vertical displacement, resulting in additional straining actions on the girder as

Fig. 13 Time history of the stress in cable 10

(a) Displacement under cable 10

(b) Displacement under cable 13
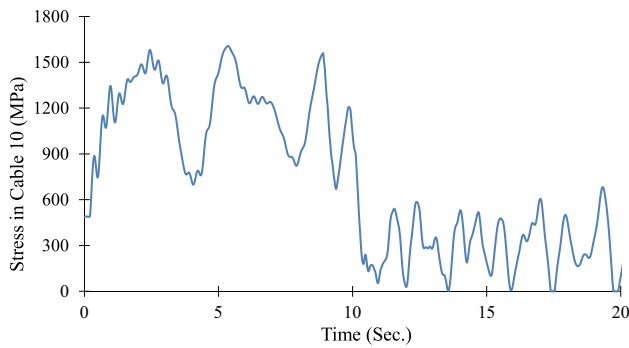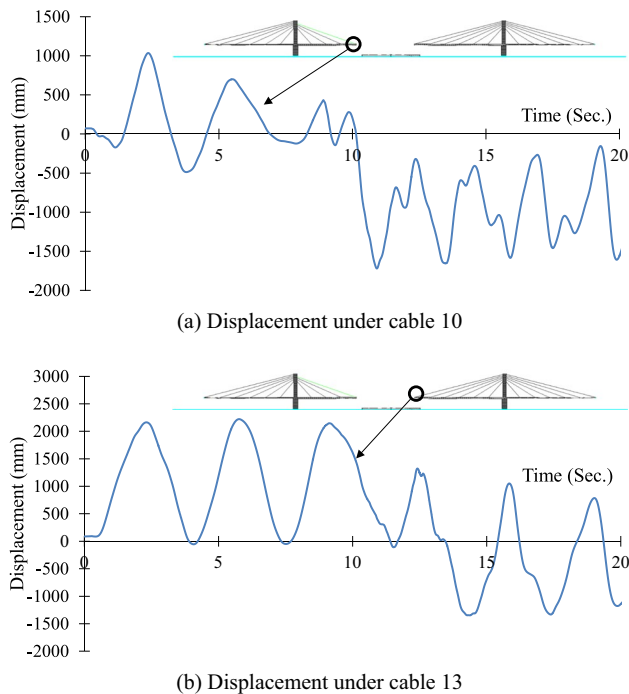
Fig. 14 Time-history of displacement at the extremities of both portions of non-collapsed decks (displacement is positive when it moves downward)

well as a significant amount of axial tension the neighboring cables.

2. Plastic hinges have been formed at the two ends of the girder, between cables 10 and 13, and in the mid-span region.

3. Moving onto cable 10, the cable has been exposed to higher values of tensile force after the cables' loss (after 0.20 s), resulting in the attainment of the yield stress at 2.4 s, as shown in Fig. 13.

4. The bridge girder has suffered more severe damage until the portion at the anchoring joint collapsed, causing downward movement of this segment. Moreover, the

stress in cable 10 has started to decrease as a result of the reduction in the applied vertical load at 10 s.

5. When this segment collided with the ground, the other portion of the girder at the anchorage joint with cable 13 collapsed, causing this segment to fall.

6. The bridge has behaved as two cantilever parts, providing an alternative load path, and therefore, the progressive collapse process has stopped.

From Fig. 12, it can be seen that the proposed modeling technique has proven to be an effective tool for analyzing the overall performance of cable-stayed bridges from early loading to ultimate collapse. This approach examines the structure's stability in a reasonably basic and effective manner. Furthermore, the study provides a clear graphic representation of the progressive collapse phenomenon.

6 Conclusions

A numerical simulation analysis based on the IAEM has been provided to facilitate the modeling of cable-stayed bridges. The fundamental benefit of the proposed model is that it can give a thorough analysis and visualization of structural behavior throughout various loading stages, ranging from modest displacement in the elastic mode to element separation and structural collapse. For that, a new type of spring element has been introduced to simulate the stay-cable as a single straight spring element with an equivalent modulus of elasticity that incorporates the effects of material and geometric deformation of the bridge cables. Moreover, the advantage of the multi-layered element has been used for modeling the pylon and the deck. In addition, an initial loading step has been implemented to consider the pretension forces in the stay-cables. During this load step, an initial strain is produced in the stay-cable to represent the prestressing forces. Furthermore, a new connection element type has been introduced to simulate the pylon-deck connection. In order to identify the essential properties of a cable-stayed bridge, the mass matrix has been modified to account for the mass of the cable-stay that is needed to apply at certain DOFs. Verification examples have been provided to test the model's functionality. A comparison of the proposed modeling technique's results with the finite element results and previous research works has revealed good agreement, showing the proposed modeling technique's reliability. Additionally, the proposed model has been examined under an extreme loading scenario represented by the simultaneous rupture of two stay-cables. The proposed modeling technique has demonstrated a strong capability to study the total performance of the cable-stayed bridges from the early stage of loading until the total collapse. This approach provides a

relatively simple and effective method to examine the stability of the structure.

7 Recommendations for Further Research

The proposed approach restricts the modeling of cable-supported bridges to straight cables with an equivalent modulus of elasticity. As a result, the current numerical model can be extended to simulate other cable configurations by dividing the cable into several straight elements in order to accurately model the curved geometry of the cable, such as in the case of a suspension bridge.

Declarations

Conflict of interest The authors declare no conflict of interest, financial or otherwise.

References

Abdelaziz MM, El-Ghazaly HA, Gomaa MS (2021a) Improved applied element model for bonded prestressed concrete structures. J Struct Eng 147:4020298

Abdelaziz MM, El-Ghazaly HA, Gomaa MS (2021b) Numerical simulation of unbonded prestressed concrete beams using improved applied element method. Eng Struct 245:112962

Abdelaziz MM, Gomaa MS, El-Ghazaly HA (2022) Progressive collapse analysis of prestressed concrete girder bridges using improved applied element method. Adv Bridg Eng 3:1–15

Abdelaziz MM, El-Ghazaly HA, Gomaa MS (2023) Performance of prestressed girders under blast loading: a probabilistic approach. Asian J Civ Eng 2023:1–12

Abdelaziz MM, El-Ghazaly H, Gomaa MS (2020) Modelling of prestressed concrete girders using improved applied element method. In: 7th Int Conf Integrity-Reliability-Failure pp 505–506

Abdel-Ghaffar AM, Nazmy AS (1991) 3-D nonlinear seismic behavior of cable-stayed bridges. J Struct Eng 117:3456–3476

Cai J, Xu Y, Zhuang L, Feng J, Zhang J (2012) Comparison of various procedures for progressive collapse analysis of cable-stayed bridges. J Zhejiang Univ Sci A 13:323–334

Cheung MS, Chidiac SE, Li W (1996) Finite strip analysis of bridges. CRC Press

CSI (Computers and Structures Inc.) (2020) SAP2000 V20 Analysis Reference Manual. CSI, Berkeley

Das R, Pandey AD, Mahesh MJ, Saini P, Anvesh S et al (2016) Progressive collapse of a cable stayed bridge. Procedia Eng 144:132–139

Das R, Pandey AD, Soumya MMJ, Anvesh S (2016) Progressive Collape vulnerability of a cable stayed bridge. Int J Bridg Eng 4:73–91

Deng L, Wang W, Yu Y (2016) State-of-the-art review on the causes and mechanisms of bridge collapse. J Perform Constr Facil 30:4015005

Domaneschi M, Cimellaro GP, Scutiero G (2019) Disproportionate collapse of a cable-stayed bridge. Proc Inst Civ Eng Eng 172:13–26

Domaneschi M, Pellecchia C, De Iuliis E, Cimellaro GP, Morgese M, Khalil AA et al (2020) Collapse analysis of the Polcevera viaduct by the applied element method. Eng Struct 214:110659

El-Kholy SA, Gomaa MS, Akl AY (2012) Improved applied element simulation of RC and composite structures under extreme loading conditions. Arab J Sci Eng 37:921–933

Elkholy S, Meguro K (2004) Numerical simulation of high-rise steel buildings using improved applied element method. In: 13th World Conf Earthq Eng, Vancouver, BC, Canada

Ernst H (1965) The modulus of elasticity of cable taking into account of catenary action. Der Bauingenieur 40:52–55

Guo X, Zhang C, Chen Z (2020) Dynamic performance and damage evaluation of a scoured double-pylon cable-stayed bridge under ship impact. Eng Struct 216:110772

Lin K, Xu Y-L, Lu X, Guan Z, Li J (2021) Collapse prognosis of a long-span cable-stayed bridge based on shake table test and nonlinear model updating. Earthq Eng Struct Dyn 50:455–474

Lin K, Xu Y-L, Lu X, Guan Z, Li J (2021) Digital twin-based collapse fragility assessment of a long-span cable-stayed bridge under strong earthquakes. Autom Constr 123:103547

Malomo D, Scattarreggia N, Orgnoni A, Pinho R, Moratti M, Calvi GM (2020) Numerical study on the collapse of the Morandi bridge. J Perform Constr Facil 34:4020044

Meguro K, Tagel-Din HS (2002) Applied element method used for large displacement structural analysis. J Nat Disaster Sci 24:25–34

Menegotto M, Pinto PE (1973) Method of analysis for cyclically loaded R. C. plane frames including changes in geometry and non-elastic behavior of elements under combined normal force and bending. Proc IABSE Symp Resist Ultim Deform Struct Acted by Well Defin Loads 1973:15–22

Mudragada R, Mishra SS (2021) Effect of blast loading and resulting progressive failure of a cable-stayed bridge. SN Appl Sci 3:1–26

Naji A, Ghiasi MR (2019) Progressive collapse analysis of cable-stayed bridges. J Fail Anal Prev 19:698–708

Nuti C, Briseghella B, Chen A, Lavorato D, Iori T, Vanzi I (2020) Relevant outcomes from the history of Polcevera Viaduct in Genova, from design to nowadays failure. J Civ Struct Heal Monit 10:87–107

Okamoto H, Maekawa K (1991) Nonlinear analysis and constitutive models of reinforced concrete. Gihodo Shuppan Company

Samali B, Aoki Y, Saleh A, Valipour H (2015) Effect of loading pattern and deck configuration on the progressive collapse response of cable-stayed bridges. Aust J Struct Eng 16:17–34

Scattarreggia N, Galik W, Calvi PM, Moratti M, Orgnoni A, Pinho R (2022) Analytical and numerical analysis of the torsional response of the multi-cell deck of a collapsed cable-stayed bridge. Eng Struct 265:114412

Scattarreggia N, Orgnoni A, Pinho R, Moratti M, Calvi GM (2023) Failure analysis of the impact of a falling object on a bridge deck. Eng Fail Anal 148:107229

Wang X, Zhu B, Cui S (2017) Research on collapse process of cable-stayed bridges under strong seismic excitations. Shock Vib 2017

Wolff M, Starossek U (2009) Cable loss and progressive collapse in cable-stayed bridges. Bridg Struct 5:17–28

Zheng Y, Wu H, You X, Xie H (2022) Model updating-based dynamic collapse analysis of a RC cable-stayed bridge under earthquakes. Structures 43:1100–1113